ARTICLES

The Mechanism of Surface Electron Ejection by Laser Excited Metastable Molecules

S. Altunata, K. L. Cunningham, M. Canagaratna, R. Thom, and R. W. Field*

Massachusetts Institute of Technology, Department of Chemistry and George R. Harrison Spectroscopy Laboratory, Cambridge, Massachusetts 02139

Received: June 12, 2001; In Final Form: November 20, 2001

Surface Electron Ejection by Laser Excited Metastables (SEELEM) is a useful but poorly understood form of laser excitation spectroscopy, whereby nominally forbidden transitions that result in the excitation of molecules into long-lived, electronically excited states are selectively (and sensitively) detected. When a molecule in a metastable (lifetime > 100 μs) electronically excited state impacts a metal surface, an electron is ejected and detected, provided that the vertical electronic excitation energy exceeds the work function of the metal. The interaction between the excited molecule and metal surface is sensitively dependent on extrinsic and intrinsic factors, such as, respectively, metal surface contamination and whether the electronic deexcitation is electron spin-allowed or forbidden. SEELEM spectra of acetylene in the region of the $\tilde{A}\ ^1A_u \leftarrow \tilde{X}\ ^1\Sigma_g^+$ ($S_1 \leftarrow S_0$) $V^3{}_0K^1{}_0$ band illustrate the effects of detector surface contamination on the relative detectivities of S_1, T_3, and T_1 electronic states on Au ($\Phi = 5.1$ eV), Y ($\Phi = 3.1$ eV), and Cs ($\Phi = 2.1$ eV) surfaces. Deexcitation via a spin-allowed transition is shown to be much more robust with respect to surface contamination than a spin-forbidden deexcitation. When the metal surface is contaminated by adsorbed acetylene, the efficiency of SEELEM detection is significantly reduced, and the surviving detectivity derives from the minuscule fractional S_1 character in predominantly T_1 eigenstates. When the SEELEM surface is less contaminated, the relative detectivities and spectral profiles on Au, Y, and Cs surfaces reflect the ~1000 times larger density of T_1, T_2 than S_1, T_3 vibrational states.

I. Introduction

Triplet states play an important role in the intramolecular energy redistribution of isolated molecules and in photochemical reactions. The chemical and structural properties of triplet states are profoundly different from those of the electronic ground state, the singlet S_0 state. Their metastability (radiative lifetime $\tau > 100\ \mu$s), electronic energy content (≥ 2 eV or 50 kcal/mol), open-shell electronic structure, and capability of existing in multiple isomeric forms combine to make triplet states potentially important in many chemical reaction processes, especially those initiated by ultraviolet radiation, electron−molecule and ion−molecule collisions, or hypersonic collisions with unexcited molecules and solid surfaces. However, despite the practical and fundamental importance of triplet states, the investigation of their structural, dynamical, and chemical kinetic properties has been limited due to the low oscillator strength of $T \leftarrow S_0$ transitions and the low spontaneous fluorescence decay rates of the triplet states.

The study of triplet states has picked up new momentum following the introduction of supersonic beam techniques, which enable the interrogation of the intramolecular dynamics of cold isolated molecules excited to well-defined quantum states. The pioneering work on the dynamics of triplet states in beams was conducted by Smalley and co-workers.[1−3] They generated triplet states, either by direct $T \leftarrow S_0$ optical excitation via the singlet character "borrowed" from energetically remote perturbers or indirectly via an intersystem crossing (ISC) process after direct optical excitation of a singlet state. They monitored the rate of decay of triplet population into high vibrational levels of the ground singlet state with an ionization laser pulse delayed with respect to the excitation laser pulse. The ionization pulse had sufficient energy to ionize any population in triplet states, but not sufficient energy to cause ionization from the high vibrational levels of the ground state. By changing the delay between the ionization and the excitation pulse, they were able to measure rates of ISC between triplet states and the high vibrational levels of the ground singlet state. The method of delayed ionization has since been used to determine rates of ISC in a wide range of molecules.[1−7]

Other experimental schemes for the detection of triplet states in molecular beams include Suzuki et al. and Ito and co-workers' method of sensitized phosphorescence,[8−13] Villa et al.'s method of multiphoton ionization,[14] Pratt and co-workers,[15−18] Penner et al.,[19] and Villa et al.'s[20] use of laser induced phosphorescence to monitor the direct excitation of large molecules to their triplet states. More recently, Sneh and Cheshnovsky introduced a new technique for the investigation of "dark" metastable molecules produced via radiationless processes following excitation by laser light.[21−30] Their technique is based on the phenomenon of electron ejection from low work-function surfaces induced by excited molecules. Sneh and Cheshnovsky report that surface electron ejection by laser excited metastables

* Author to whom correspondence should be addressed.

10.1021/jp012219l CCC: $22.00
Published on Web 01/24/2002

(SEELEM) yields results in good agreement with those obtained from delayed ionization experiments in the determination of the decay rates of triplet states of large molecules.[21] They have also shown that SEELEM detection sensitivity is independent of excess vibrational energy in the triplet state.[21] The basic idea behind SEELEM had actually been developed by Klemperer, Freund, and co-workers[31,32] for the detection of metastables generated by electron impact in effusive beams. Sneh and Cheshnovsky enhanced the power of this method by replacing electron bombardment by laser excitation and by generation of triplet states via radiationless processes in a supersonic beam.

Sneh and Cheshnovsky applied SEELEM mostly to the study of triplet decay rates and the quantum efficiencies of nonradiative processes in large molecules (e.g. aniline, pyrazine). We use SEELEM to interrogate the triplet states of small polyatomic molecules (e.g. acetylene) with the goal of understanding the details of the radiationless process that transforms population into triplet states. Uncovering the mechanistic details of how triplet states are populated could lead to the development of schemes to selectively excite these states and open up possibilities of using triplet states as platforms for new kinds of spectroscopic, dynamical, external control, photochemical, and chemical kinetics experiments.

SEELEM is our primary experimental tool to investigate triplet states and, hence, it is important to characterize this detection scheme. Although there is a rich literature describing the process of deexcitation of excited atoms on impact with metal surfaces, the theory has not been fully extended to the case of $S_1 \sim T_i$ mixed molecular eigenstates (e.g. $|\Psi_{mixed}> = \alpha|\Psi_{S1}> + (1 - \alpha^2)^{1/2}|\Psi_T>$) interacting with surfaces. The seminal review of the mechanism of interaction of excited atoms with metal surfaces is by Hagstrum.[33] Silbey et al. have described the fate of an oscillating dipole in close proximity (a few Å) to a surface from a semiclassical point of view.[34] More recently Hotop has reviewed the mechanisms of the detection of metastables on surfaces.[35] Hotop demonstrates that the detection mechanism and efficiency are intimately linked to the condition of the detector surface.

A comparison of the data we have acquired in two molecular beam machines with different base pressures has led us to conclude that the quantum efficiency of SEELEM detection of a metastable state that has predominantly dark state (T) character derives from its minuscule bright state (S_1) character if the SEELEM surface is contaminated by adsorbates. This is due to the fact that deexcitation via a spin-allowed transition takes place through a long-range interaction and, hence, is more robust with respect to surface contamination. However, if the SEELEM surface conditions are improved, the short-range tunneling interaction channel, which allows spin-forbidden deexcitation, is opened and the dark character of the metastables can be detected as well.

In this paper we report our findings that demonstrate the critical dependence of the efficiency of the SEELEM process for triplet and singlet fractional characters of mixed molecular eigenstates on extrinsic factors such as the background pressure during detection. We propose that at sufficiently low background pressures, where the short-range interaction pathway is not suppressed, SEELEM on low-work function metals such as Cs ($\Phi_{Cs} = 2.1$ eV) can be exploited as a sensitive method to detect the triplet fractional characters of mixed molecular eigenstates. Being sensitive to the triplet fractional character of an eigenstate, as opposed to being limited to detecting exclusively its fractional bright state character, opens up the possibility of being able to observe nominally "dark" eigenstates excited in direct triplet−singlet transitions and determine the fractional S_1, excited triplet, and lowest triplet characters in each eigenstate. This distribution of eigenstate characters will provide a fundamental understanding of the mechanisms of excitation, ISC, and detection.

II. Experimental Section

SEELEM spectra are recorded in a second-generation version of an apparatus described previously.[36,37] The first-generation molecular beam machine, in which the SEELEM spectra displayed as Figure 3 were acquired, consisted of a single vacuum chamber that contained two detectors: a photomultiplier tube (PMT) and a SEELEM detector. The operating pressure in this chamber was 2×10^{-5} Torr. The current apparatus is a doubly differentially pumped vacuum chamber, where the operating pressure in the "detector" compartment that houses the SEELEM detector is 4×10^{-7} Torr.

A 1 atm mixture of C_2H_2 (Matheson) seeded in He (BOC Gases) in a 1:5 ratio is expanded through a 0.5 mm diameter pulsed nozzle (Jordan Valve, open time 35 μs), operated at 10 Hz, into vacuum as a freely expanding jet. The unskimmed molecular jet is crossed 1.5 cm downstream from the nozzle by laser light linearly polarized parallel to the molecular beam propagation direction. A Nd:YAG pumped, frequency doubled dye laser (5 ns pulse duration, tuned between 225 and 215 nm, 300 μJ pulse energy, 3 mm diameter, 0.08 cm^{-1} spectral full width at half-maximum (fwhm)), excites the $\tilde{A} \leftarrow \tilde{X}$ $V^3_0K^1_0$ transition of $^{12}C_2H_2$. (Here V stands for the trans bending mode and K stands for the projection of **J**, the total angular momentum, along the *a*-axis.) The background pressure in the "source" chamber with the nozzle operating is 2×10^{-5} Torr, as it was in the first-generation chamber. A PMT and a Ge detector (Edinburgh Instruments) directly view the excitation region and collect the UV (200 to 300 nm) and IR (700 nm to 1.8 micron) components of the fluorescence, respectively. UV-laser induced fluorescence spectra and IR-laser induced fluorescence spectra are recorded simultaneously with SEELEM spectra; however, these photon-detected spectra will not be discussed in this paper. At a point 1.5 cm downstream from the excitation region, the molecular beam, now containing laser excited metastables, passes through a 3-mm diameter electroformed skimmer (Precision Instruments) into the detector chamber where the operating pressure is 4×10^{-7} Torr. The excited molecules travel another 5−25 cm before colliding with the SEELEM detector. The SEELEM detector comprises a metal surface and an electron multiplier. On impact with the SEELEM detector surface, the metastable molecules are deexcited and the deexcitation energy causes electrons to be ejected from the metal surface. These electrons are captured by the electron multiplier (ETP, SGE Instruments, 10^5 gain) and counted by a multichannel scaler (Oxford Instruments).

The distance from the excitation region to the SEELEM surface is variable and permits measurement of the lifetimes of the metastable molecules. The measured lifetimes of the SEELEM detected eigenstates excited in the vicinity of the $\tilde{A} \leftarrow \tilde{X}$ $V^3_0K^1_0$ band cluster around 60 μs, with the states associated with the R(1) rotational transition ($J' = 2 \leftarrow J'' = 1$) exhibiting the longest lifetimes at ~100 μs. Lifetime measurements are more accurately performed in the second-generation apparatus because the collimation of the molecular beam brought about by the presence of the skimmer, ensures that all the photoexcited molecules in the supersonic molecular beam are captured on the active surface of the SEELEM detector (a circle of radius 1 cm situated between 15 and 25 cm from the nozzle, which

corresponds to a 0.014−0.005 sr solid angle relative to the nozzle orifice).

Another important variable in the experiment is the metal used as the SEELEM detector surface. The use of different metals as the SEELEM detector surface (Au, Ag, Cu, Y, Sm, Cs) permits variation of the relative sensitivities to $T_{1,2}$ vs T_3 excited triplet electronic states because the conversion of the electronic energy of an electronically excited metastable state to an ejected electron occurs only if the vertical electronic deexcitation energy exceeds the work function of the SEELEM metal (eq 1)

$$E_k = E_{T_i} - \Phi_{metal}$$

$$E_k > 0 \text{ if } E_{T_i} > \Phi_{metal} \qquad (1)$$

where E_k is the kinetic energy of an ejected electron, E_{T_i} is the vertical electronic energy of the state T_i, and Φ_{metal} is the work function of the metal. Neither excess vibrational excitation nor translational energy contributes significantly to SEELEM detectivity.[22,33,38]

III. Results and Discussion

An expression for the intensities in the SEELEM spectrum has been proposed previously,[36,37]

$$I_i^{SEELEM} = C_{S_1}{}^2 \times [e^{-\Delta t \times \gamma}] \times (C_{S_1} + \alpha C_{T_i})^2 \qquad (2)$$

where γ is the decay rate via spontaneous emission given by $\gamma = (1/0.27\ \mu s) \times C_{S_1}{}^2$. The flight time, Δt, may be changed between 94 and 156 μs for a 20% mixture of C_2H_2 seeded in He by varying the distance from the excitation region to the SEELEM surface. The intrinsic lifetime of a pure singlet eigenstate is 0.27 μs.[36] C_{S_1} and C_{T_i} denote the singlet (bright) and triplet (dark) amplitudes of the mixed molecular eigenstates created upon laser excitation. The SEELEM detectivity expression is a product of three factors: (1) the excitation probability (the fractional bright state character of each mixed molecular eigenstate), $C_{S_1}{}^2$; (2) the probability of surviving the flight time, Δt, from excitation until impact on the detector while *preserving the electronic excitation*, which is also determined by the fractional S_1 character, $C_{S_1}{}^2$; (3) the SEELEM detectivity, which is related to the square of the weighted sum of the amplitudes of the basis states that lie at vertical electronic excitation energies larger than the work function of the SEELEM metal. For example, in the case of Au (Φ = 5.1 eV), only the S_1 and T_3 basis state characters are detectable. However, when Cs (Φ = 2.1 eV) is used as the SEELEM detector surface, all electronically excited states of acetylene, including T_1, contribute to the detectivity, at least in principle. Whether one achieves the expected increase in SEELEM signal strength due to turning on the detectivity of a higher density of excited triplet vibrational states is shown here to depend crucially on the background pressure at which the SEELEM measurement is made. Figure 1 compares the energies of the electronic states of acetylene to the work functions of some of the metals used as SEELEM surfaces.

Because S_1 and T_i represent electronic surfaces with different total electron spin, their intrinsic SEELEM detectivities are not expected to be identical. Therefore, a phenomenological scaling factor, α, was inserted into the detectivity factor of the SEELEM expression (eq 2). Most experimental studies of the interaction mechanisms of electronically excited gaseous species with metal surfaces have involved atoms. It is known that an atom in an

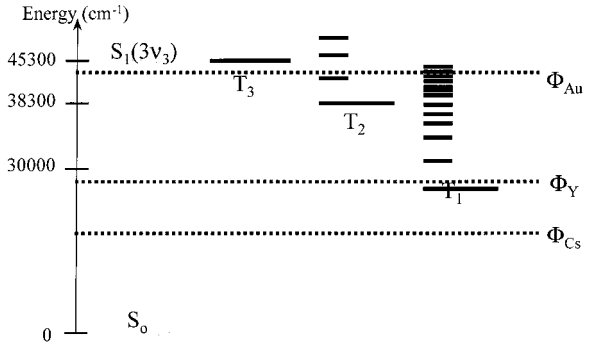

Figure 1. Schematic of the energy levels of acetylene and the work functions of the SEELEM metals used to probe the populations in these levels.

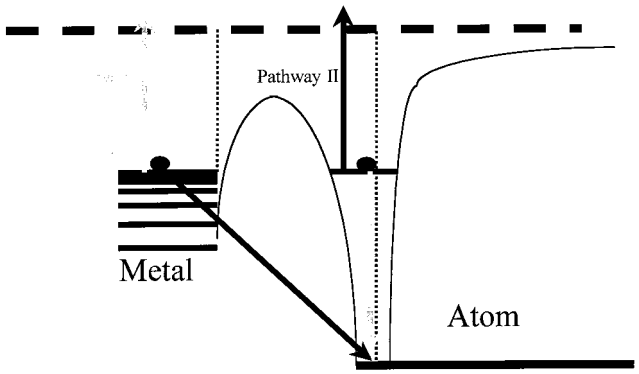

Figure 2. Two mechanisms of the deexcitation of an electronically excited atom on impact with a metal surface. The upper horizontal dashed line represents the energy of a free electron. The two vertical dotted lines define the distance from the metal surface at which the excited atom starts to interact with the metal (a few angstroms). Pathway I, represented by the gray arrowheaded lines, involves ejection of an electron from the conduction band of the metal by the energy released when the excited electron in the atom relaxes to the ground state. In pathway II, represented by the black arrowheaded lines, an electron from the conduction band of the metal falls into the half filled orbital of the atom causing the excited electron on the atom to be ejected. Pathway II is very similar to the more commonly known ionization pathway, which involves transfer of the excited electron to the metal in cases where the excited electron orbital lies above the Fermi level of the metal. This figure was inspired by Figure 1 in a paper by Homer D. Hagstrum published in 1954 (*Phys. Rev.* **1954**, *96*(2), 325).

electronically excited singlet state can give rise to electron ejection on impact with a metal surface through two pathways.[33] In the first pathway, the excited electron of the atom relaxes to fill the vacancy in the lowest unfilled atomic orbital, whereupon the energy released by this deexcitation causes an electron to be ejected from the conduction band of the metal (Figure 2). In the second pathway, an electron from the conduction band of the metal tunnels through a barrier into the vacancy in the lowest energy unfilled atomic orbital, thereby causing the excited electron on the atom to be ejected. (Another pathway very similar to pathway II described here is known as the ionization pathway. If the excited electron orbital lies above the Fermi level of the metal, the excited electron may transfer to the metal.) This is followed by neutralization of the resulting ion in an Auger-like process and ejection of a surface electron. The ionization pathway will not be considered separately since it also involves exchange of electrons between the excited atom and the metal. For an electronically excited atom in a triplet state, the first of these two signal pathways is not viable since it would require a spin flip of the excited electron as it relaxes into the singlet ground state. Extending this picture to the case of S ~ T mixed

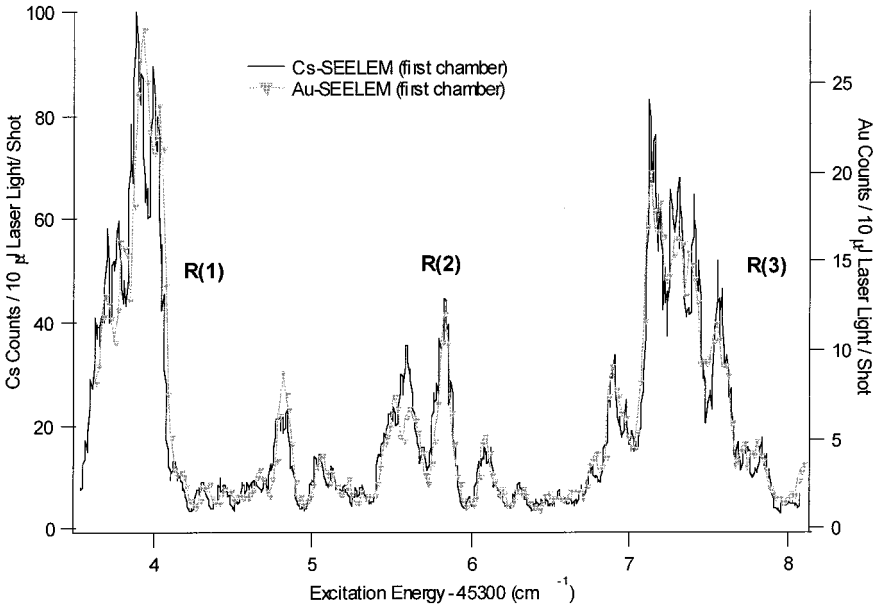

Figure 3. SEELEM spectra of a section of the $\tilde{A} \leftarrow \tilde{X}$ $V^3_0K^1_0$ band of acetylene centered near 220.74 nm. The SEELEM traces were acquired on either Cs ($\Phi = 2.1$ eV) or Au ($\Phi = 5.1$ eV). These spectra were acquired in the first-generation chamber where the operating base pressure was 2×10^{-5} Torr.

eigenstates, it is reasonable to expect that for a mixed state with comparable fractional SEELEM-detectable singlet and triplet characters, the SEELEM detectivity arising from the fractional singlet character would be larger than that arising from the triplet character. Hence, it is appropriate to incorporate a phenomenological scaling factor into the SEELEM signal expression to account for this expected difference in the S_1 vs T_i detectivities.

For the SEELEM processes described by Figure 2, pathway I can be considered as a "long-range interaction" pathway. The singlet character of S∼T mixed eigenstates can deexcite through this singlet-only pathway, resulting in the emission of an electron. Pathway II, which is the only viable pathway for the deexcitation of the triplet character, is a "short-range interaction" or "tunneling" pathway since it requires overlap between the orbitals of the mixed molecular state and the orbitals of the metal conduction band. The short-range interaction pathway should be more sensitive to the cleanliness of the SEELEM surface and, hence, the background pressure. In fact, the short-range interaction pathway can shut down under high background pressures.[35] This would result in a further reduction of the detectivity for the triplet character of a mixed molecular eigenstate relative to that for the singlet character. The efficiency of the SEELEM process for the triplet character relative to the singlet character is likely to depend sensitively on the background pressure, and this dependence is additional motivation for the introduction of the empirical parameter, $\alpha(P)$, into the SEELEM intensity expression.

The form of the detectivity factor (eq 2) suggests that quantum interference effects between the contributions of different classes of basis states will be a characteristic (and perhaps diagnostically useful) feature of SEELEM spectra, especially when the eigenstate density exceeds the spectral resolution. Collision with the SEELEM surface could induce inelastic transitions among eigenstates, which would reduce or eliminate the expected interference structures in SEELEM spectra. However, in the limit where the density of SEELEM nondetectable basis states is vastly in excess of the SEELEM detectable ones, inelastic collisions with the SEELEM surface are not expected to alter the spectrally averaged SEELEM detectivity, but should smooth out the sharp structures associated with constructive/destructive interference.

Figure 3 shows two overlaid SEELEM spectra corresponding to a section of the R-branch region of the $\tilde{A} \leftarrow \tilde{X}$ $V^3_0K^1_0$ band of acetylene. These spectra were recorded in the first-generation apparatus where the background pressure was 2×10^{-5} Torr during detection. The SEELEM spectrum displayed as a darker line was recorded on Au ($\Phi = 5.1$ eV); and the SEELEM spectrum shown as a light line was recorded on Cs ($\Phi = 2.1$ eV). Despite the high background pressure, the Au spectrum recorded compares very well with corresponding Au spectra obtained by Wodtke et al. at a lower resolution in a doubly differentially pumped vacuum system where the detection chamber background pressure was 5×10^{-7} Torr.[36] The Au and Cs detection surfaces in the first-generation apparatus were both located 10 cm from the excitation region. The Au surface was heated to 300 °C while the spectrum was recorded, in an attempt to minimize the buildup of physisorbed acetylene on the metal surface. Cs was continuously coated onto a rotating copper wheel while the spectrum was recorded. Coating was done at the upper half of the copper wheel while the metastables impacted the lower half. The wheel was rotating at 2 rpm and the time required for the freshly coated Cs to rotate 180° into the path of the incoming metastables was 15 s.

It is useful at this point to estimate the flux of background molecules onto the SEELEM surface at the prevailing background pressures in our first and second generation chambers. Using the kinetic theory of gases, one can calculate the number of collisions per unit area per unit time under pressure p for a gas with molar mass M. For air, at room temperature, at a pressure of 2×10^{-5} Torr, the flux of molecules is 8×10^{15} /s/cm^2. Since 1 cm^2 of metal surface consists of about 10^{15} atoms, each atom is struck about 8 times per second at this pressure. Since it takes 15 s for a fresh Cs surface to be exposed to the incoming metastables, each surface Cs atom is struck ∼120 times by background molecules before the arrival of the first signal molecules. It is difficult to estimate the fraction of collisions that gives rise to adsorption; however, if one assumes a sticking coefficient of 0.1, one finds that the time required to deposit one monolayer is 1.25 s.

If the background pressure is reduced to 4×10^{-7} Torr, as in the second-generation apparatus, the fresh Cs atoms on the

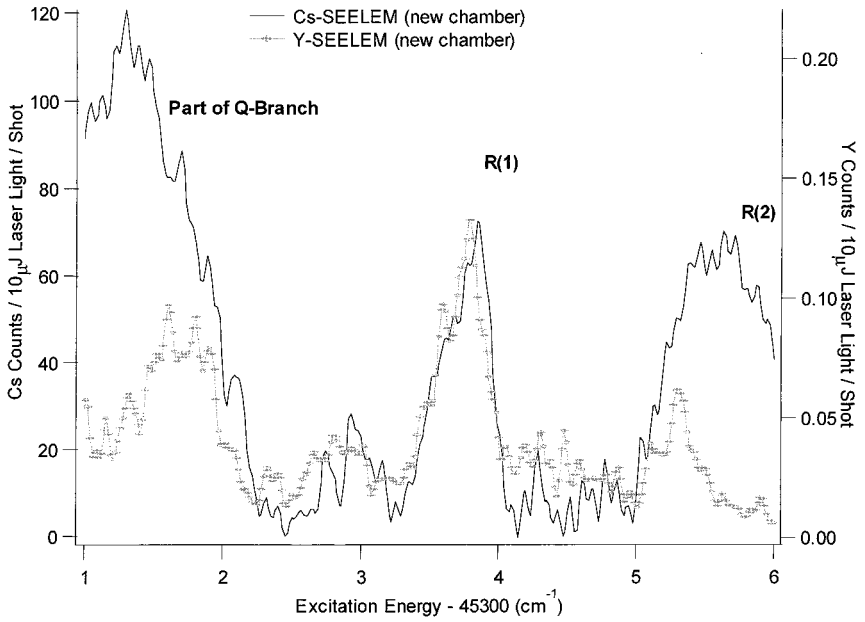

Figure 4. SEELEM spectra of a section of the $\tilde{A} \leftarrow \tilde{X}$ $V^3_0K^1_0$ band of acetylene centered near 220.74 nm. The SEELEM traces were acquired on either Cs ($\Phi = 2.1$ eV) or Y ($\Phi = 3.1$ eV). These spectra were acquired in the second generation chamber where the operating base pressure was 4×10^{-7} Torr.

SEELEM surface suffer only 2.4 collisions during the 15 s period prior to exposure to the incoming metastables. This reduction by a factor of about 50 in the number of collisions suffered by the surface atoms is likely to significantly improve the surface cleanliness and, therefore, keep the short-range interaction channel open, as required for the efficient detection of the triplet character of the metastable eigenstates.

The SEELEM spectra recorded in the first generation apparatus are surprisingly similar in their relative intensities, both feature-by-feature and overall. Au and Cs surfaces are expected to give rise to profoundly different SEELEM spectra, since these metals are capable of detecting different groups of triplet states: only the T_3 and S_1 characters of the eigenstates are detectable on Au, but T_1 and T_2 characters, in addition to the T_3 and S_1 characters, should be detectable on Cs (Figure 1). It should be noted here that the density of $T_{1,2}$ states is expected to be $\sim 10^3$ times larger than the density of S_1, T_3 states. Failure to observe the expected significant differences in the line shapes and relative intensities of the Au and Cs SEELEM spectra led us to conclude that the triplet character is much less detectable than the singlet character. This implies that the empirical parameter α in the SEELEM intensity expression (eq 2) is much smaller than 1. The Cs surface does exhibit an overall increase in the signal level by a factor of 3 relative to the Au surface; however, this is much smaller than the expected $\sim 10^3$ increase if T_1 and T_2 basis state characters had also been detectable.

Figure 4 is a comparison of two SEELEM spectra featuring a slightly different region of the R-branch of the acetylene $\tilde{A} \leftarrow \tilde{X}$ $V^3_0K^1_0$ band, recorded this time in the second-generation chamber at a background pressure of 4×10^{-7} Torr during detection. The first trace (light line) was acquired with Y ($\Phi = 3.1$ eV) as the SEELEM surface, and the second trace (dark line) was acquired with Cs ($\Phi = 2.1$ eV). The Y and Cs surfaces were both located 15 cm from the excitation region. Although these spectra are survey spectra, they clearly show that under the improved background pressure condition, the Cs signal is at least 500 times stronger (as determined by the R(1) feature) than the Y signal (which, in turn, is a factor of 3 stronger than Au), and the detailed feature shapes and relative intensities in the two spectra are significantly different. This is a profound contrast with the situation in Figure 3.

The spectra obtained in the new chamber were acquired under quite different conditions than those in the old chamber (different background pressure, different SEELEM surface to excitation distance, presence of a skimmer, different backing pressure hence a different rotational temperature of the molecular beam, a different electron multiplier, and slightly different nozzle-excitation region distance. Over time, the electron multiplier dynodes rapidly become contaminated and the gain coefficient for the ejected SEELEM electrons is reduced. Therefore, the electron multipliers are replaced approximately every six months.) Therefore, the two sets of SEELEM traces cannot be compared directly to each other, but are internally comparable.

The performance of the second-generation apparatus was tested by recording two SEELEM spectra on Au at different laser nozzle delays. The laser nozzle delay parameter is an important parameter which ensures that the laser beam passes through the excitation region precisely at the time the molecules released from the nozzle arrive there. Adjusting the laser nozzle delay permits excitation of the molecular beam at spatially different points as it traverses the laser excitation region. Each pulse of molecules can be thought of as a "rod of molecules" travelling with a Gaussian distribution of translational velocities centered around 1.6×10^5 cm/s. If the laser beam intercepts this rod of molecules at the front edge, then the leading edge of the molecular beam will be composed of excited molecules, and these molecules will collide with the clean SEELEM surface first, giving rise to SEELEM signal. However, if the laser intercepts the rod of molecules at the tail end, then the leading edge of the molecular beam will be composed of unexcited molecules, and, if not pumped away sufficiently fast, this leading edge of unexcited molecules could become adsorbed onto the SEELEM surface, rendering it less efficient at the detection of the later-arriving, tail-end, excited molecules. Alternatively, the leading edge of unexcited molecules could form a "high" pressure cloud

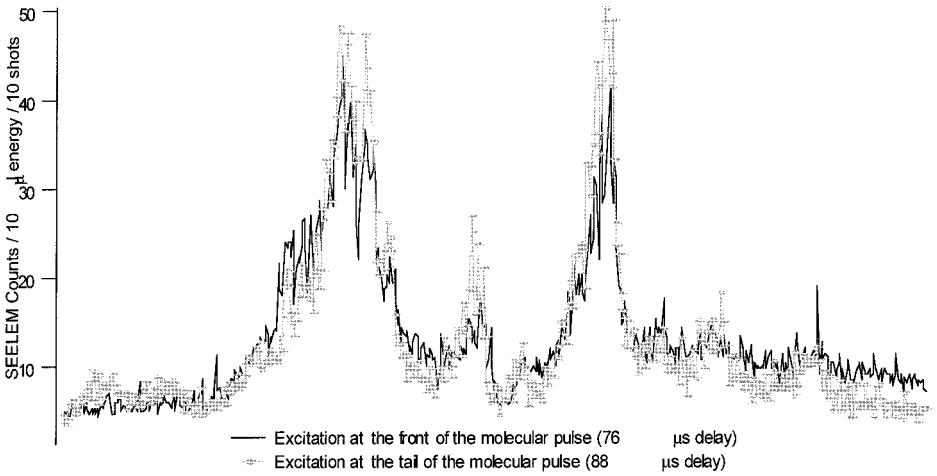

Figure 5. SEELEM spectra of a section of the $\tilde{A} \leftarrow \tilde{X}$ $V^3_0K^1_0$ band of acetylene centered near 220.74 acquired on Au in the second-generation chamber where the operating base pressure was 4×10^{-7} Torr with two different laser nozzle delays: 76 μs and 88 μs. The lack of detectable differences between the two spectra indicates that there is no significant build-up of adsorbates on the SEELEM surface during the detection process. The shorter laser nozzle delay corresponds to exciting the molecular pulse at the front end such that the excited molecules impact the SEELEM surface first. The longer laser nozzle delay corresponds to exciting the tail-end of the molecular pulse so that the excited molecules impact the SEELEM surface after the unexcited molecules in the front part of the pulse. If the unexcited molecules in the leading edge are not pumped away fast enough, they may adsorb to the SEELEM surface and reduce the detectivity of the excited molecules arriving in the tail-end of the molecular pulse.

in front of the SEELEM surface, which would cause the incoming metastable molecules to be scattered out of the beam.

A decline of SEELEM efficiency as a function of laser nozzle delay was observed in the first-generation apparatus and is diagnostic of background pressure impacting the SEELEM detectivity. However, in the second-generation apparatus, changing the laser nozzle delay by as much as 12 μs, which corresponds to a time window during which the molecular beam travels 1.9 cm, did not detectably alter the intensity profile of the SEELEM spectra (Figure 5). There is an upper limit to how much the laser nozzle delay can be increased without changing the total number of excited molecules significantly. The laser induced fluorescence was monitored in each case in this experiment to ensure that the same number of molecules were being excited. The data shown in Figure 5 were acquired with a brand new electron multiplier and, hence, are characterized by larger number of counts/laser shot than the survey spectra. The pumping in the second-generation apparatus minimizes the build-up of potential adsorbates or "scatterers" in front of the SEELEM surface, thus keeping the SEELEM surface clean for the incoming flux of excited molecules. The laser nozzle delay test proves that the superiority of the second-generation chamber at detecting the $T_{1,2}$ character of the molecular eigenstates is indeed a direct consequence of the improved background pressure and the cleaner SEELEM surface.

The survey spectra of Figure 4 clearly show that the relative intensities of the SEELEM spectra acquired on Y and Cs are profoundly different. This demonstrates conclusively that, under improved vacuum conditions, the short-range detection pathway approaches its expected efficiency, making possible direct detection of the $T_{1,2}$ character in the molecular eigenstates. The signal level on the Cs surface is also a factor of 500 greater as compared to that acquired on the Y surface (or a factor of 1500 as compared to that acquired on Au). According to Drabbels et al., the vibrational density of states of the T_1 surface at the energy of the transition being recorded in these experiments is about 10 cm^{-1},[39] which is a factor of about 1000 larger than the density of T_3 states (0.01 cm^{-1}) in this energy region. Therefore, the expected enhancement in SEELEM signal should be about 1000-fold upon switching to a metal sensitive to the $T_{1,2}$ character of the molecular eigenstates. This is in agreement with observations.

IV. Future Experiments

The enormous change in the efficiency of the short-range channel achieved by reducing the background pressure confirms our model for SEELEM detectivity and opens up the possibility of recording direct triplet excitation spectra as well as directly measuring the S_1, T_3, and $T_{1,2}$ characters in metastable eigenstates.

Zwier and co-workers have determined a peak absorption cross section of 2.7×10^{-5} atm^{-1} cm^{-1} for the direct triplet−singlet ($^3\Delta_u \leftarrow {}^1\Sigma_g^+$) transition in C_4H_2 using cavity ringdown spectroscopy.[40] They report that this transition is 3×10^6 times weaker than the strongest transition of C_4H_2, which is the $^1\Delta_u \leftarrow {}^1\Sigma_u^+$ transition. Although this suggests that the corresponding triplet−singlet transition in acetylene should also be exceedingly difficult to observe directly, we believe that the demonstrated sensitivity of SEELEM with Cs as the detection surface could make it possible to detect direct excitations to T_1, T_2, and T_3 states at energies far from resonance with S_1 vibrational levels.

We estimate the expected SEELEM signal level on Cs that would result from exciting a direct $T_1 \leftarrow S_0$ transition in C_2H_2. As shown in eq 2, the SEELEM signal arises from the contributions of three multiplicative factors: the excitation probability, the survival probability, and the detectivity. One can calculate the magnitudes of each of these factors for the case of the $S_1 \leftarrow S_0$ transition of acetylene detected on Au and compare the result to the expected magnitudes of the same factors for the case of the $T_1 \leftarrow S_0$ transition detected on Cs. Since we know the signal levels achieved when Au is used as the SEELEM surface, we can predict how difficult it would be to observe the forbidden transition in acetylene using Cs as the detector surface.

We have measured the lifetimes of the SEELEM states we observe on Au that arise from the excitation of the $S_1 \leftarrow S_0$ transition of acetylene. Based on these data, the S_1 fractional bright state character of the SEELEM states observed on Au is $\sim$0.005. The T_3 character of these SEELEM states, which is

the only other electronic state character that can give rise to signal on Au, is more difficult to calculate. However, one can estimate the T_3 character by making use of the known density of states that belong to different electronic states in the energy region of the $S_1 \leftarrow S_0$ transition and the couplings between these levels:

$$S_1 = 0.01\ \text{cm}^{-1}$$
$$T_3 = 0.01\ \text{cm}^{-1}$$
$$T_{1,2} = 10\ \text{cm}^{-1}$$
$$S_0 = 1000\ \text{cm}^{-1} \quad (3)$$

The interactions between acetylene electronic states may be ordered according to their strengths: $S_0 \sim S_1 \ll S_0 \sim T \ll S_1 \sim T \ll T_i \sim T_i$.[41] Therefore, the T_3 character will *not* be distributed democratically over all the states in this energy region. In fact, we have some results which suggest that the eigenstates observed in our experiments possess very little, if any, S_0 character: the SEELEM spectrum in the region of the $4\nu_3$ level of S_1, where ν_3 is the trans bending mode, shows no sign of predissociation, even though the S_0 surface is unbound at this energy. Therefore, it can be concluded that T_3 character fractionates predominantly into $T_{1,2}$ states. In this case, one would expect the average T_3 character of an eigenstate to be 0.01/10 or 10^{-3}. Using these numbers, one can determine that the SEELEM signal on Au for eigenstate transitions near resonant with the $S_1 \leftarrow S_0$ $V_0^3K_0^1$ band will be proportional to

$$I_{\text{Au}}^{\text{SEELEM}} = 0.005 \times [e^{(-\Delta t/0.27\mu s)\times(0.005)}] \times (\sqrt{0.005} + \sqrt{10^{-3}})^2 = 5.2 \times 10^{-5} \times e^{-\Delta t/0.27\mu s} \quad (4)$$

For the purposes of this calculation, α (eq 2) is assumed to be unity.

A similar analysis can be carried out for the case of direct $T_1 \leftarrow S_0$ excitation detected on Cs. The first factor, which is the excitation probability, will be proportional to the minuscule S_1 fractional bright state character acquired through spin−orbit mixing with the energetically remote S_1 state. The nature of the spin−orbit interaction that couples states of different multiplicity is discussed by El-Sayed.[42] The magnitude of the $S_1 \sim T_1$ spin−orbit coupling in C_2H_2 has been calculated as 1.6 cm^{-1} by Cui et al.[43] This is to be contrasted with the 13.7 cm^{-1} calculated coupling between S_1 and T_3.[43] The transition probability for a nominally triplet state, ν_t, can be calculated as follows:

$$|\langle \nu_x|\mu|\nu_t\rangle|^2 = |\langle \nu_x|\mu|\left(\left|\nu_t^0\right\rangle + H_{\text{el}}\sum_{\nu_s^0}\frac{\langle \nu_s^0|\nu_t^0\rangle}{E_{\nu_t^0} - E_{\nu_s^0}}\left|\nu_s^0\right\rangle\right)|^2$$
$$\cong |\langle \nu_x|\mu|\left(\frac{H_{\text{el}}}{E_{\text{T}} - E_{\text{S}}}\sum_{\nu_s^0}\langle \nu_s^0\left|\nu_t^0\right\rangle \left|\nu_s^0\right\rangle\right)|^2$$
$$= \frac{H_{\text{el}}^2\mu_{sx}^2}{(E_{\text{T}} - E_{\text{S}})^2}\left(\sum_{\nu_s^0}\langle \nu_x|\nu_s^0\rangle\langle \nu_s^0|\nu_t^0\rangle\right)^2$$
$$= \frac{H_{\text{el}}^2}{(E_{\text{T}} - E_{\text{S}})^2}\mu_{sx}^2 q\nu_t^0\nu_x \quad (5)$$

In the above equation, H_{el} denotes the electronic part of the spin−orbit coupling matrix element between S_1 and T_1, which is the quantity calculated by Cui et al,[43] and ν_x is the initial vibrational state of S_0. The vibrationally excited S_0 states were not included in the expansion of the nominally triplet eigenstate, ν_t, since the coupling between S_0 and T is predicted to be much weaker than that between S_1 and T.[41] The dependence of the denominator of the perturbation theoretic expansion of $|\nu_t\rangle$ on the vibrational levels of S_1 was also ignored for simplicity. The energy denominator was factored out of the summation expression, and completeness was used to collapse the sum over ν_s^0 to yield a (ν_t^0, ν_x) vibrational overlap factor. The S_1 trans minimum lies at 45 301 cm^{-1},[39] and the T_1 trans minimum lies at 39 360 cm^{-1}.[44] The fractional S_1 bright state character of the eigenstate ν_t is then given by

$$|\langle \nu_x|\mu|\nu_t\rangle|^2 = C_{S_1}^2 \times \mu_{sx}^2 \times q\nu_t^0\nu_x$$
$$C_{S_1}^2 \cong \frac{H_{\text{el}}{}^2}{(E_{\text{T}} - E_{\text{S}})^2}$$
$$C_{S_1}^2 \cong \frac{1.6^2}{5941^2} \quad (6)$$

The fractional S_1 character in ν_t is 7.3×10^{-8}. However, there is one more parameter to consider in order to properly evaluate the strength of the $T_1 \leftarrow S_0$ ($\nu = 0$) transition with respect to that of the $S_1(\nu_3 = 3) \leftarrow S_0(\nu = 0)$ transition: Watson's calculations of the vibrational intensities in the $\tilde{A}-\tilde{X}$ electronic transition of acetylene show that the vibrational overlap factor for the $\nu_3' - 0$ progression increases rapidly with increasing number of quanta of excitation in the upper state up to a maximum increase of a factor of 300 relative to the $1\nu_3' - 0$ band.[45] This trend can be expected to occur in the T_1 electronic state as well since, according to ab initio calculations, the shapes of the S_1 and T_i potential surfaces resemble each other.[46] Therefore, the vibrational overlap factor in the intensity expression for the $T_1 \leftarrow S_0$ ($\nu = 0$) transition can be increased by at least a factor of 10 relative to the vibrational overlap factor for the S_1 ($\nu_3 = 3$) $\leftarrow S_0$ ($\nu = 0$) transition by targeting high vibrational levels ($\nu \geq 5$) of the T_1 surface.

The detectivity term in the SEELEM expression in the case of direct T−S excitation will be estimated as 1 since this is approximately the average fractional triplet state character acquired by an eigenstate in the energy region of the direct T−S transition. Fractionation of the triplet character over S_0 states is again assumed to be negligible.[41]

Evaluating the SEELEM expression for the direct T−S excitation case, one finds that the SEELEM signal on Cs will be proportional to

$$I_{\text{Cs}}^{\text{SEELEM}} = \left(\frac{1.6\ \text{cm}^{-1}}{5941\ \text{cm}^{-1}}\right)^2 \times [e^{-(\Delta t/0.27\mu s)\times 7.3\times 10^{-8}}] \times 1 \times 10$$
$$= 7.3 \times 10^{-7} \times e^{-(\Delta t/0.27\mu s)} \quad (7)$$

where the last factor of 10 is the vibrational overlap enhancement factor for the Franck−Condon strong $T_1 \leftarrow S_0$ ($\nu = 0$) transition relative to the S_1 ($\nu_3 = 3$) $\leftarrow S_0$ ($\nu = 0$) transition.

The important parameters that play a role in the Au/Cs signal comparison calculation are summarized in Table 1. The intensity of the $T_1 \leftarrow S_0$ ($\nu = 0$) transition is estimated to be a factor of 70 weaker than that of the S_1 ($\nu_3 = 3$) $\leftarrow S_0$ ($\nu = 0$) transition. The *optimized* signal from S_1 $3\nu_3$ acquired on Au is typically 10 counts/shot/100 μJ of laser light. We have observed weaker

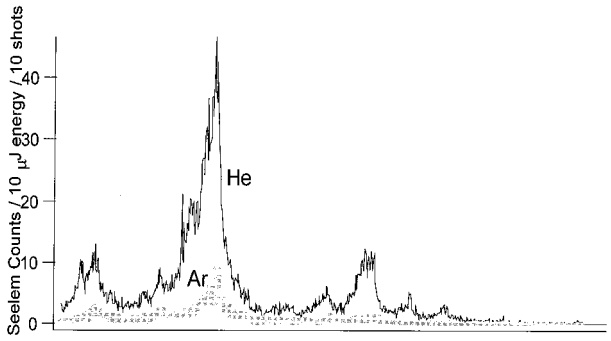

Figure 6. SEELEM spectra of a hot band transition ($V_1^3K_1^0$) of C_2H_2 acquired on Au in the second-generation apparatus. The molecules were seeded in Ar and He. Ar is much more efficient at vibrational cooling, hence the reduction in signal due to the reduction of population in the ground state in the case of Ar as the carrier gas. The efficiency of Ar at vibrational cooling could be exploited in distinguishing hot band transitions from other weak, cold band transitions, such as direct T ← S_0 excitations.

TABLE 1: Au/Cs Signal Comparison Calculation Parameters

SEELEM surface	Au	Cs
fractional S_1 character	0.005	7.3×10^{-8}
detectivity	$(\sqrt{0.005} + \sqrt{10^{-3}})^2$	1
Franck−Condon enhancement	1	10
signal level	5.2×10^{-5}	7.3×10^{-7}
signal level normalized with respect to Au	1	1/70

signals on Au. These were axis-switching transitions and their intensity was about 0.2 counts/shot/100 μJ of laser light. Although it is possible to observe signal on Au, which is a factor of 50 smaller than the "reference" S_1 $3\nu_3$ signal, the S/N ratio associated with the Cs surface is much poorer than the one associated with Au and, therefore, it could be difficult to detect signal on Cs that is a factor of 70 less than the reference S_1 $3\nu_3$ signal. However, it is possible to improve the S/N ratio on Cs by increasing data collection time, decreasing the background pressure in the chamber, and by suppressing ejection of "thermal" electrons from the Cs surface. The background pressure in the chamber could be improved by subjecting the chamber to an extensive pumping cycle. The ejection of thermal electrons from the Cs surface could be suppressed by cooling the Cs surface. Alternatively, one could choose to improve the S/N ratio by increasing the signal level. This could be achieved by increasing the laser intensity or the concentration of acetylene in the molecular beam.

Another challenge associated with recording direct T−S excitation spectra is distinguishing these forbidden transitions from others such as hot band transitions. One signature of T−S transitions will be absence of detectable fluorescence signal. However, there is another way to determine whether a certain signal arises from a T−S transition or a hot band S_1 ← S_0 transition: We have shown that Ar as a carrier gas is very efficient at vibrational cooling. He, on the other hand, was shown to be efficient only at rotational cooling. We have recorded two spectra of the $V_1^3K_1^0$ transition of acetylene (S_1 ← $S_{0(hot)}$) using He and Ar as the carrier gases (Figure 6). As the spectra show, the signal level goes down by a factor of 5 due to vibrational cooling when Ar is used as the carrier gas. Therefore, to distinguish hot band transitions from transitions originating from $\nu = 0$, one would compare spectra recorded with Ar and He carrier gas.

There are some results from electron-energy loss studies that predict the energies of the strongest vibrational bands for the T ← S_0 transitions of C_2H_2.[44,47−49] Guided by these predictions, we expect to be able to record T ← S_0 SEELEM excitation spectra of acetylene.

V. Conclusion

We have demonstrated the profoundly different effects of detector surface contamination on S_1 vs T detectivity in surface electron ejection by laser excited metastables (SEELEM) spectroscopy. SEELEM is a powerful technique that has been used to study the triplet states of molecules. It involves emission of electrons from metal surfaces upon impact by excited metastable species. The efficiency of the SEELEM process depends critically on the background pressure. The deexcitation of a mixed molecular eigenstate upon impact with a SEELEM surface can proceed through two pathways, known as the short-range and long-range interaction pathways. The triplet character of the eigenstates deexcites exclusively through the short-range interaction pathway. This pathway is very sensitive to the cleanliness of the SEELEM surface. At high background pressures, the short-range interaction pathway is shut down, leading to very inefficient detection of the triplet character relative to the singlet character of the eigenstates. We have shown that, by improving the vacuum conditions, one drastically alters the efficiency of the SEELEM process and enhances the triplet-detection channel.

This is the first step in constructing a mechanistic picture of the SEELEM detection process. The dependence of detectivity both on extrinsic (background pressure) and intrinsic (electronic state composition of the metastable eigenstates) parameters needs to be explicitly considered in the interpretion of the SEELEM spectra to draw accurate conclusions about the fundamental intramolecular energy redistribution processes that give rise to the metastable states being detected.

The next barrier that must be overcome before dynamically meaningful spectra can be obtained is spectral resolution. We hope to achieve a factor of 20 higher resolution than the present 0.08 cm^{-1} in our next phase experiments. Higher resolution spectra will allow us to effectively use the analytical tools we have developed[37,50] to uncover the mechanism governing the redistribution of energy in our model system.

Acknowledgment. This project has been supported by the Air Force Office of Scientific Research (AFOSR), grants No.F49620-97-1-0040 and AASERT F49620-97-1-0384.

References and Notes

(1) Duncan, M. A.; Dietz, T. G.; Liverman, M. G.; Smalley, R. E. *J. Chem. Phys.* **1981**, *85*, 7.
(2) Dietz, T. G.; Duncan, M. A.; Smalley, R. E. *J. Chem. Phys.* **1982**, *76*, 1227.
(3) Dietz, T. G.; Duncan, M. A.; Pulu, A. C.; Smalley, R. E. *J. Chem. Phys.* **1982**, *86*, 4026.
(4) Smalley, R. E. *J. Phys. Chem. A* **1982**, *86*, 3504.
(5) Otis, C. E.; Knee, J. L.; Johnson, P. M. *J. Chem. Phys.* **1983**, *78*, 2091.
(6) Sur, A.; Johnson, P. M. *J. Chem. Phys.* **1986**, *84*, 1206.
(7) Knee, J. L.; Johnson, P. M. *J. Chem. Phys.* **1984**, *80*, 13.
(8) Suzuki, T.; Shi, Y.; Kohguchi, H. *J. Chem. Phys.* **1997**, *106*, 5292.
(9) Shi, Y.; Suzuki, T. *J. Phys. Chem. A* **1998**, *102*, 7414.
(10) Abe, H.; Kamei, S.; Mikami, N.; Ito, M. *Chem. Phys. Lett.* **1984**, *109*, 217.
(11) Kamei, S.; Mikami, N.; Ito, M. *J. Chem. Phys.* **1986**, *90*, 2321.
(12) Kamei, S.; Okuyamam, K.; Abe, H.; Mikami, N.; Ito, M. *J. Chem. Phys.* **1986**, *90*, 93.
(13) Ohmori, N.; Suzuki, T.; Ito, M. *J. Chem. Phys.* **1988**, *92*, 1086.
(14) Villa, E.; Terazima, M.; Lim, E. *Chem. Phys. Lett.* **1986**, *129*, 336.
(15) Spangler, L. H.; Matsumoto, Y.; Pratt, D. W. *Phys. Chem.* **1983**, *87*, 4781.
(16) Spangler, L. H.; Pratt, D. W. *J. Chem. Phys.* **1986**, *84*, 4789.

(17) Spangler, L. H.; Pratt, D. W.; Birss, F. W. *J. Chem. Phys.* **1986**, *85*, 3229.
(18) Tomer, J. L.; Holtzclaw, K. W.; Pratt, D. W. *J. Chem. Phys.* **1988**, *88*, 1528.
(19) Penner, A.; Oreg, Y.; Villa, E.; Lim, E. C.; Amirav, A. *Chem. Phys. Lett.* **1988**, *150*, 243.
(20) Villa, E.; Amirav, A.; Lim, E. C. *Chem. Phys. Lett.* **1988**, *147*, 43.
(21) Sneh, O.; Amirav, A.; Cheshnovsky, O. *J. Chem. Phys.* **1989**, *91*, 7154.
(22) Sneh, O.; Cheshnovsky, O. *J. Phys. Chem. A* **1991**, *95*, 7154.
(23) Sneh, O.; Cheshnovsky, O. *Chem. Phys. Lett.* **1986**, *130*, 53.
(24) Sneh, O.; Cheshnovsky, O. *Chem. Phys. Lett.* **1988**, *146*, 216.
(25) Sneh, O.; Cheshnovsky, O. *Chem. Phys. Lett.* **1986**, *130*, 487.
(26) Sneh, O.; Cheshnovsky, O. *Isr. J. Chem.* **1990**, *30*, 13.
(27) Sneh, O.; Dünn-Kittenplon, D.; Cheshnovsky, O. *J. Chem. Phys.* **1989**, *91*, 7331.
(28) Becker, I.; Cheshnovsky, O. *J. Chem. Phys.* **1994**, *101*, 3649.
(29) Cheshnovsky, O.; Amirav, A. *Chem. Phys. Lett.* **1984**, *109*, 368.
(30) Sneh, O.; Cheshnovsky, O. *J. Chem. Phys.* **1992**, *96*, 8095.
(31) Freund, R. S.; Klemperer, W. *J. Chem. Phys.* **1967**, *47*, 2897.
(32) Hemminger, J. C.; Wicke, B. G.; Klemperer, W. *J. Chem. Phys.* **1976**, *65*, 2798.
(33) Hagstrum, H. D. *Phys. Rev.* **1954**, *96*, 325.
(34) Chance, R. R.; Prock, A.; Silbey, R. *Adv. Chem. Phys.* **1978**, *37*, 1.
(35) Hotop, H. *Exp. Methods Phys. Sci.* **1996**, *29*.
(36) Humphrey, S. J.; Morgan, C. G.; Wodtke, A. M.; Cunningham, K. L.; Drucker, S.; Field, R. W. *J. Chem. Phys.* **1997**, *107*(1), 49.
(37) Altunata, S.; Field, R. W. *J. Chem. Phys.* **2000**, *113*, 6640.
(38) Lisy, J. M.; Klemperer, W. *J. Chem. Phys.* **1980**, *72*, 3880.
(39) Drabbels, M.; Heinz, J.; Meerts, W. L. *J. Chem. Phys.* **1994**, *100*(1), 165.
(40) Hagemeister, F. C.; Arrington, C. A.; Giles, B. J.; Quimpo, B.; Zhang, L.; Zwier, T. S. In *Cavity Ring-down Spectroscopy: An Ultratrace-Absorption Measurement Technique*; Busch, K. S., Busch, M. A., Eds.; ACS number 720; Oxford University Press: U.K., 1999; pp 210−232.
(41) Dupré, P.; Green, P. G.; Field, R. W. *Chem. Phys.* **1995**, *196*, 211.
(42) El Sayed, M. A. *Acc. Chem. Res.* **1968**, *1*, 8.
(43) Cui, Q.; Morokuma, K.; Stanton, J. F. *Chem. Phys. Lett.* **1996**, *263*, 46.
(44) Swiderek, P.; Michaud, M.; Sanche, L. *J. Chem. Phys.* **1997**, *106*, 9403.
(45) Watson, J. K. G. *J. Mol. Spectrosc.* **2001**, *207*, 276.
(46) Ochi, N.; Tsuchiya, S. *Chem. Phys.* **1991**, *152*, 319.
(47) Wendt, H. R.; Hippler, H.; Hunziker, H. E. *J. Chem. Phys.* **1979**, *70*, 4044.
(48) Wilden, D. G.; Hicks, P. J.; Comer, J. *J. Phys. B: Atom. Mol. Phys.* **1977**, L403.
(49) Hammond, P.; Jureta, J.; Cvejanović, D.; King, G. C.; Read, F. H. *J. Phys. B: At. Mol. Opt. Phys.* **1987**, *20*, 3547−3556.
(50) Altunata, S.; Field, R. W. *J. Chem. Phys.* **2001**, *114*, 6557.